

See discussions, stats, and author profiles for this publication at: <https://www.researchgate.net/publication/231673996>

Nanoparticles of Polyampholyte–Surfactant Complexes with Perfluorododecanoic Acid

ARTICLE *in* LANGMUIR · APRIL 2002

Impact Factor: 4.46 · DOI: 10.1021/la020067v

CITATIONS

8

READS

11

3 AUTHORS, INCLUDING:



Andreas F Thünemann

Bundesanstalt für Materialforschung und -pr...

178 PUBLICATIONS **4,968** CITATIONS

SEE PROFILE



Ulrich Wendler

Fraunhofer Institute for Applied Polymer Res...

12 PUBLICATIONS **245** CITATIONS

SEE PROFILE

Nanoparticles of Polyampholyte–Surfactant Complexes with Perfluorododecanoic Acid

Andreas F. Thünemann,* Ulrich Wendler, and Werner Jaeger

Fraunhofer Institute for Applied Polymer Research, Geiselbergstrasse 69,
D-14476 Golm, Germany

Heimo Schnablegger

Institut für Physikalische Chemie, Universität Hamburg, Bundesstrasse 45,
D-20146 Hamburg, Germany

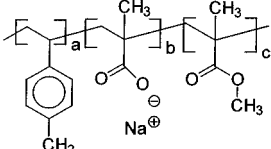
Received January 18, 2002. In Final Form: February 20, 2002

Polyampholytes were synthesized and complexed with perfluorododecanoic acid. This produces highly fluorinated water-soluble nanoparticles, which are long-term stable. The polyampholytes are copolymers of styrylmethyl(trimethyl)ammonium chloride, methacrylic acid, and methyl methacrylate having more cationic monomers (28–100 mol %) than anionic monomers (0–16%). The cationic monomers form a complex with perfluorododecanoate ions to create neutral entities that aggregate while the negatively charged methacrylic monomers prevent a macroscopic precipitation such as normally observed in fluorinated complexes. Negatively charged nanoparticles, which have ζ potentials of about -40 mV, are formed as a result of the combined complexation and stabilization. Small-angle X-ray scattering investigations reveal that the particles are anisotropic. For example, disk-shaped particles with a diameter of $D \geq 30$ nm and a height of 2.2 nm were formed for a high number of complexing groups (79 mol %). Cylindrical-shaped particles with lengths of $H \geq 25$ nm and radii of 1.5 nm were produced for a medium number of complexing groups (57 mol %). Fluorescence spectroscopy with pyrene as the probe was used to determine the critical aggregation concentrations of the particles which are in the range 0.01 – 0.06 g L $^{-1}$.

Introduction

The stoichiometric 1:1 complexation of polyelectrolytes with oppositely charged surfactants typically results in the formation of water-insoluble soft-matter materials with numerous interesting liquid crystalline-like phases that have been reviewed by Zhou and Chu¹ and Ober and Wegner² as well as Tirrell et al.³ For clarity, the stoichiometry is always calculated with respect to the charges. In contrast to stoichiometric, nonstoichiometric polyelectrolyte–surfactant complexes are often water soluble due to excess charges that stabilize the aggregates of the complexes.⁴ For example, we investigated the complexes of high molecular weight poly(ethylene imine) and dodecanoic acid. It forms a water-insoluble solid-state complex with a smectic A-like structure with a 1:1 stoichiometry.⁵ The same complex with an excess of poly(ethylene imine) of 50 mol % forms nanoparticles of a core-shell type that are useful as carriers of lipophilic drugs such as Q₁₀ and triiodothyronine.⁶

The aim of the work presented here was to complex polyampholytes with perfluorododecanoic acid to form highly fluorinated nanoparticles that are stable in aqueous solutions. Ternary polyampholytes with cationic, anionic, and neutral monomers seemed to be suitable for this



	monomers in mol %	a (cationic)	b (anionic)	c (neutral)
complex C ₂₈	28	08	64	
complex C ₅₇	57	16	27	
complex C ₇₉	79	13	08	
complex C ₁₀₀	100	-	-	

Figure 1. Chemical structures and composition of the polyampholyte–perfluorododecanoate complexes C₂₈, C₅₇, C₇₉, and C₁₀₀.

purpose. Styrylmethyl(trimethyl)ammonium chloride was chosen as the complexing cationic monomer, methacrylic acid as the stabilizing anionic monomer and methyl methacrylate as the “charge-diluting” neutral monomer. Perfluorododecanoic acid was chosen because it had already been shown to be suitable for the formation of complexes with homopolymers.⁷ The chemical structures of the complexes are shown in Figure 1. Their preparation and nanoparticle formation include the following steps: (1) synthesis of noncharged precursor polymers; (2) quaternization and partially saponification of the precursor polymers to polyampholytes, where the precursor route makes it possible to determine the molecular weight and weight distribution of the polyampholytes with a high degree of accuracy, which is otherwise a difficult problem; (3) Complexation of the polyampholytes with dodecanoic acid and simultaneously their dispersion to nanoparticles.

(7) Thünemann, A. F. *Langmuir* 2000, 16, 824–828.

* Corresponding author. E-mail: andreas.thuenemann@iap.fhg.de.

(1) Zhou, S. Q.; Chu, B. Assembled materials: Polyelectrolyte-surfactant complexes. *Adv. Mater.* 2000, 12, 545–556.

(2) Ober, C. K.; Wegner, G. *Adv. Mater.* 1997, 9, 17–31.

(3) MacKnight, W. J.; Ponomarenko, E. A.; Tirrell, D. A. *Acc. Chem. Res.* 1998, 31, 781–788.

(4) Goddard, E. D.; Ananthapadmanabham, K. P., Eds. *Interaction of Surfactants with Polymers and Proteins*; CRC Press: Boca Raton, FL, 1993.

(5) Thünemann, A. F.; General, S. *Langmuir* 2000, 16, 9634–9638.

(6) Thünemann, A. F.; General, S. *J. Controlled Release* 2000, 75, 237–247.

Table 1. Composition of the Complexes and Characteristics of the Nanoparticles: ζ Potentials, Shape, and Size as Determined by SAXS and the Hydrodynamic Diameters as Determined by DLS

complex	monomers (mol %)			ζ potential (mV)	structure	size (SAXS) (nm)	D_H (DLS) (nm)
	cationic	anionic	neutral				
C ₂₈	28	08	64	-41 \pm 7	different shaped particles	20–30	21 \pm 8
C ₅₇	57	16	27	-38 \pm 4	cylindrical particles	$H \geq 25$ $R = 1.5 \pm 0.1$	25 \pm 5
C ₇₉	79	13	08	-40 \pm 2	disk-shaped particles	$H = 2.2 \pm 0.1$ $D \geq 30$	34 \pm 5
C ₁₀₀	100			no particles	smectic A-like mesophase	long period $L = 3.4$	

Experimental Section

Materials. The surfactant used in this study, perfluorododecanoic acid, was supplied by Fluka and used in the state as received. It had a melting point of 108 °C that is close to the melting point reported by Zisman et al.⁸ (101–106 °C). The water was from a Milli-Q system. Commercially available vinylbenzyl chloride was delivered by Dow which is a mixture of 70 mol % meta and 30 mol % para isomers. It was purified prior to its use by extraction with sodium hydroxide solution (10 g L⁻¹) and fractionated distillation (64 °C, 0.3 mbar). The methyl methacrylate was supplied by Aldrich. The dibenzoyl peroxide was supplied by Merck and purified by precipitating it from a saturated dried chloroform solution with methanol.

Synthesis of Polyampholytes. Precursor Synthesis. The synthesis of poly(vinylbenzyl chloride-co-methyl methacrylate) was carried out by free radical polymerization reaction using dioxane as a solvent in a such a way that the degree of polymerization was about 500. To achieve this, the total concentration of the monomers had to be 4.0 mol L⁻¹. Fractions of 12, 25, 50, and 100 mol % vinylbenzyl chloride monomers were used in the reaction mixture. The initiating concentration of dibenzoyl peroxide was 0.02 mol L⁻¹. The polymerization was carried out for a reaction time of 90 min at a temperature of 70 °C in an argon atmosphere. The polymers were then precipitated from the reaction mixture by using methanol and purified by precipitation in butanone. ¹H NMR spectroscopy was used to determine the composition of the poly(vinylbenzyl chloride-co-methyl methacrylate)s which showed vinylbenzyl chloride fractions of 28, 57, 79, and 100 mol %, respectively. Gel permeation chromatography (eluent: THF) calibrated with polystyrene standards was used for the molecular weight determination, which showed $M_n = 43\,000$, 42 500, 40 000, 50 000. The polydispersities were $M_w/M_n = 1.72$, 1.62, 1.69, 1.69. The glass transition temperatures of the polymers were determined to be 110, 101, 92, and 77 °C by using differential calorimetry.

Polyampholyte Synthesis. The chlormethyl functions of the precursors were transformed to methyl(trimethyl)ammonium functions by using trimethylamin in a heterophase reaction. By analogy to the procedure described earlier,⁹ the water insoluble precursors were dispersed in aqueous solutions of trimethylamin (20% (w/w)) and reacted at 100 °C during boiling. Homogeneous solutions of quaternization products were obtained after 60 min. Purification was carried out by ultrafiltration (the molecular weight membrane cutoff was 3000) and isolation by freeze-drying. ¹H NMR spectroscopy revealed that the chlormethyl groups were converted quantitatively to methyl(trimethyl)ammonium groups; i.e., the cationic groups were 28, 57, 79, and 100 mol %. A partially saponification of the ester groups of the methyl methacrylate monomers to carboxylic acid groups was obtained during the reaction conditions applied. The ratio of methyl methacrylate to methacrylic acid groups was determined using IR spectroscopy. In combination with the results from the ¹H NMR spectroscopy gave the composition of the polyampholytes (cf. Figure 1 and Table 1). It can be seen there that the anionic groups were in the range 0–16 mol %.

Complexation and Nanoparticle Formation. For the complex preparation, 100 mg of polyampholyte was dissolved in 100 mL of water and heated to 90 °C. An 1.05 equiv of

perfluorododecanoic acid was dispersed in 100 mL of hot water (90 °C), adjusted to a pH of 7 by using sodium hydroxide and then stirred for 30 min. As a result an opaque viscous dispersion of sodium perfluorododecanoate was obtained. The stoichiometry was calculated with respect to the number of ammonium groups of the polyampholytes and perfluorododecanoate moieties. The solutions of the polymers were added dropwise to dispersions of the perfluorododecanoate to form the complexes C₂₈, C₅₇, C₇₉, and C₁₀₀. The subscripts indicate the amount of cationic monomers of the polyampholytes. Transparent solutions of complexes were obtained for C₂₈, C₅₇, and C₇₉ while the complex C₁₀₀ precipitates spontaneously.

Methods. The size of the nanoparticles was determined by dynamic light scattering, using a fixed angle (90°) Nicomp 370 submicrometer particle sizer. The samples were loaded into the measuring cell at concentrations in the range 0.1–1% (w/w). The intensity-averaged size was derived by using the Nicomp distribution analysis provided by version 12.0 of the Nicomp software. The number of replications was five. The ζ potentials of the nanoparticles were determined with a Zetamaster (Malvern Instruments) averaging five measurements. The same solutions were used for dynamic light scattering and ζ potential measurements.

We performed the small-angle X-ray scattering experiments with a Kratky compact camera (Anton Paar, Austria), equipped with a stepping motor and a counting tube with an impulse-height discriminator. The light source was a conventional X-ray tube with a fixed copper target operating at 40 mA and 30 kV. No monochromator (except the built-in impulse-height discriminator of the detector) was used. Instead, the $K\beta$ contributions were numerically calculated in the subsequent desmearing procedure which is included in the program ITP^{10–12} that transforms the scattering data into real space and gives the radial pair-distance distribution functions (PDDF). This program uses the equation

$$I_D(q) \propto \int_{r=0}^{\infty} p(r) \frac{\sin qr}{qr} dr \quad (1)$$

where $p(r)$ is the radial PDDF to be calculated and $I_D(q)$ the desmeared scattering intensity as a function of q . The scattering vector is defined in terms of the scattering angle θ and the wavelength λ of the radiation (Cu K α = 0.154 nm) thus

$$q = \frac{4\pi}{\lambda} \sin(\theta/2) \quad (2)$$

The actual experimental data $I(q)$ can be expressed in terms of the desmeared intensity $I_D(q)$ (see eq 7 in ref 11) and both functions, $p(r)$ and $I_D(q)$, were computed in one step using the experimental scattering function $I(q)$, the wavelength-distribution data and the corresponding beam-profile of the experimental equipment. The temperature of the sample was adjusted to 25 \pm 1 °C using a K-HR temperature controller (Anton Paar, Austria). The luminescence of pyrene in the dispersions of the nanoparticles was analyzed using a Perkin-Elmer LS-50B luminescence spectrometer. Emission spectra collected were in the range 350–500 nm with an excitation wavelength of 330 nm

(8) Hare, E. F.; Shafrin, E. G.; Zisman, W. A. *J. Colloid Sci.* **1954**, *58*, 236–239.

(9) Wendler, U.; Bohrisch, J.; Jaeger, W.; Rother, G.; Dautzenberg, H. *Macromol. Rapid Commun.* **1998**, *19*, 185–19.

(10) Glatter, O. *Acta Phys. Austriaca* **1977**, *47*, 83.

(11) Glatter, O. *J. Appl. Crystallogr.* **1977**, *10*, 415.

(12) Glatter, O. *J. Appl. Crystallogr.* **1979**, *12*, 166.

and slits of 2.5/2.5 nm. The concentrations of the pyrene was 10^{-7} mol L $^{-1}$.

Results and Discussion

The macroscopic behavior of the complexes C_{28} , C_{57} , and C_{79} is quite different from that of C_{100} . The former dissolve transparently in water while the latter precipitates to a soft matter as is normally found for stoichiometric complexes of fluorinated amphiphiles and oppositely charged polyelectrolytes.^{13,14} The C_{100} forms, for example, surfaces with Zisman critical surface tension¹⁵ ($\gamma_c < 20$ mN/m) when cast to form free-standing films. Hexadecane, tetradecane, dodecane and decane were used as test liquids for contact angle measurements. Equidistant reflections in the small-angle X-ray pattern of C_{100} indicate that it has a lamellar structure with a long period of $L = 3.4$ nm (not shown). This dimension is in agreement with a noninterdigitated tail-to-tail arrangement of the carboxylate moieties with their heads linked by polyelectrolyte chains. This lamellar structure of C_{100} is within our expectation due to what is normally observed for complexes of fluorinated carboxylic acids.^{16,17} Major reasons for the dominance of lamellar structures are that the phase behavior of single-chain perfluorinated carbon acids is characterized by the formation of disk-shaped micelles in low concentrations^{18,19} and further that the lamellar phase often borders on the isotropic micellar solution.¹⁸ For this reasons it is surprising that the complexes C_{28} , C_{57} , and C_{79} form transparent, optically homogeneous solutions. The solutions of C_{57} and C_{79} are long-term stable at room temperature (for longer than 6 months) while that of C_{28} becomes opaque, and finally, some precipitate is observed after storage times of only 2 weeks. The precipitate of the C_{28} complex can be dissolved by heating the solution to 80 °C and keeping it at that temperature for half an hour. Then, after it was returned to room temperature, slow precipitation starts again after several days.

The reason for the absence of a spontaneous precipitation after complex formation in the cases of the complexes of C_{28} , C_{57} , and C_{79} seems to be a result of the ampholytic character of the polymers. C_{57} and C_{79} have 16 and 13 mol % carboxylate groups respectively, which cause the long-term stabilization of the complex solutions. In contrast C_{28} has only 8 mol % carboxylate groups, which produce stabilization for only periods of several days. C_{100} precipitates immediately because it has no stabilizing groups.

As it was important to determine whether discrete particles of complexes or molecular aggregates were formed, dynamic light scattering and small-angle X-ray scattering were carried out.

Nanoparticles. The dynamic light scattering measurements of the complexes revealed that the complexes form discrete nanoparticles with hydrodynamic diameters of 21 ± 8 (C_{28}), 25 ± 5 (C_{57}), and 34 ± 5 nm (C_{79}). In contrast to their complexes, the dynamic light scattering data of the neat polyampholytes indicate scattering objects with hydrodynamic diameters smaller than 10 nm. Therefore, the presence of aggregates of the polyampholytes, due to intermolecular salt formation, can be ruled out.

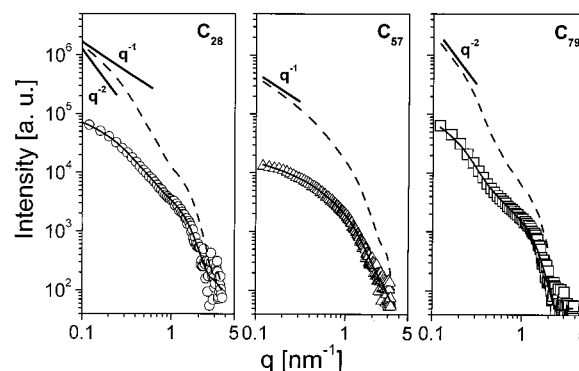


Figure 2. Small-angle X-ray scattering curves obtained for a 1% (w/w) aqueous solution of the complexes C_{28} , C_{57} , and C_{79} . The symbols represent the data points as measured with a Kratky camera. The solid lines represent the fits to the experimental data obtained by a Fourier transformation of the pair distance distribution function in Figure 3. The dashed lines represent the desmeared scattering curves as calculated from data taking into account the geometry of the beam and the wavelength distribution. The slopes of q^{-1} are indicated to emphasize the region of the scattering of cylindrical particles and q^{-2} for that of the disklike particles.

The ζ potentials of the particles were measured and found to be very similar: -41 ± 7 (C_{28}), -38 ± 4 (C_{57}), and -40 ± 2 mV (C_{79}) (cf. Table 1). This proves that the particles are electrically stabilized and all the ζ potentials are sufficiently low to provide (from the viewpoint of electrical stabilization) a long-term stability.

A more detailed investigation of the particles was carried out by small-angle X-ray scattering. The measurements of aqueous solutions of the dispersed complexes were investigated at concentrations in the range 0.2–2% (w/w), and the shape of the scattering curves did not change significantly within this range. From this we concluded that the scattering entities in the solution do not change significantly or cluster. In contrast, the shape of the scattering curves of the different complexes differ significantly. Examples are shown in Figures 2. The scattering intensities are plotted as a function of the scattering vector, q . Here it can be seen that the scattering intensities decrease monotonically with increasing value of q and further that the envelope of the intensity decays 3–4 orders of magnitude, as expected for particles in dilute systems. For monodisperse particles, the intensity is expected to oscillate at larger q values while a distribution of particle sizes result in a reduction of the oscillations, but the envelope should not be affected.

Of interest is the geometry of the particles in solution. Therefore, a quantitative evaluation of the scattering data was carried out by the indirect Fourier transform method as developed by Glatter.^{11,20} This method transforms the experimental scattering function into pair-distance distribution functions, $p(r)$, where smearing effects from the beam geometry and the wavelength distribution are already taken into account. The desmeared scattering intensities are shown in Figure 2 (dashed curves) and the $p(r)$ in Figure 3.

Slopes of q^{-1} and q^{-2} that are characteristic for a cylindrical shape and a disklike shape, respectively, are indicated in Figure 2. From this it is obvious that the shapes of the nanoparticles must be different. The scattering curve of C_{28} decays with a noninteger slope at a small scattering vector that is between q^{-1} and q^{-2} (Figure 2, left-hand side). The shape of the C_{28} particles is probably ill-determined. Presumably this sample con-

(13) Antonietti, M.; Henke, S.; Thünemann, A. *Adv. Mater.* **1996**, *8*, 41–45.

(14) Thünemann, A. F. *Polym. Int.* **2000**, *49*, 636–644.

(15) Zisman, W. A. *Ind. Eng. Chem.* **1963**, *55*, 18.

(16) Thünemann, A. F. *Langmuir* **2000**, *16*, 824–828.

(17) Thünemann, A. F.; Stephan Kubowicz, S.; Pietsch, U. *Langmuir* **2000**, *16*, 8562–8567.

(18) Hoffmann, H. *Ber. Bunsen-Ges. Phys. Chem.* **1984**, *88*, 1078.

(19) Holmes, M. C.; Reynolds, D. J.; Boden, N. *J. Phys. Chem.* **1987**, *91*, 1, 5257–5262.

(20) Glatter, O. *J. Appl. Crystallogr.* **1980**, *13*, 577.

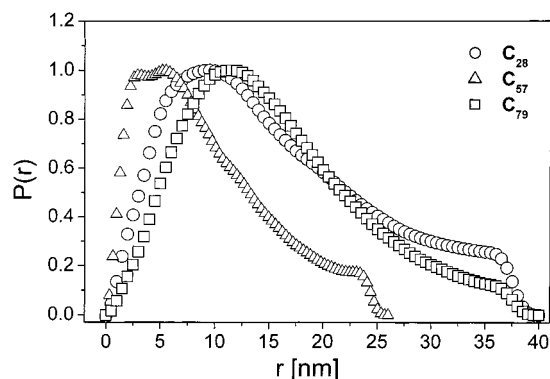


Figure 3. Pair distance distribution functions $p(r)$ of C_{28} (circles), C_{57} (triangles), and C_{79} (squares) obtained from the indirect Fourier transformation of the scattering intensities in Figure 2. The pair distance distribution function of C_{28} is not characteristic of a defined shape of the particles. In contrast, the $p(r)$ of C_{57} indicates a cylindrical shape and the $p(r)$ of C_{79} indicates a disklike shape.

sists of a mixture of cylindrical and disklike particles, so that slope considerations are no longer valid. In contrast, the intensity for C_{57} decays along the line of q^{-1} for low values of q (Figure 2, middle). This is characteristic of rodlike particles. Further, the decay of the intensity of C_{79} is as q^{-2} which is indicative for disklike particles (Figure 2, right).

All of the pair-distribution functions in Figure 3 have a tail toward large r , which indicates elongated particle shape (cf. Glatter et al. and literature therein²¹). The $p(r)$ of C_{57} is indicative for elongated cylindrical particles (Figure 3, triangles) and that of C_{79} for flat disklike particles (squares) while that of C_{28} (circles) is not characteristic of particles with a simple geometry (cf. Glatter et al. and literature therein²¹). Most likely, the particles of C_{28} are not uniform in their geometry. From the linear extrapolations of the pair distribution functions in Figure 3 (not shown) the axial lengths of the cylinders were determined to be $H \geq 25$ nm, the diameters of the disks were $D \geq 30$ nm and the size of the C_{28} particles was ≥ 30 nm. These values are in good agreement of the results from the dynamic light scattering data. It must be said that the $p(r)$ values are cut off at the large r value side, because the scattering functions were experimentally accessible only down to $q = 0.1 \text{ nm}^{-1}$ which does not allow for a calculation of the $p(r)$ values at distances larger than 32 nm.

The $p(r)$ in Figure 3 are not very sensitive to variations in the smaller extensions of the particles, i.e., the diameters of the cylinders and the height of disks. This is not necessarily a problem in the interpretation process, especially when the basic geometry, such as cylindrical or lamellar geometry are known. In these cases, the scattering functions can be split up into two parts, one coming from the infinite extent of the cylinder or lamella and the other coming from the density distribution of the cross-section perpendicular to the cylinder axis or to the lamellar surface. Presuming that the cylinder's height is much larger than its diameter, the cross-section distribution function for the cylinder,^{20,21} $p_c(r)$, can be calculated by the inversion of

$$q I(q) \propto \int_0^\infty p_c(r) J_0(qr) dr \quad (3)$$

(21) Iampietro, D. J.; Brasher, L. L.; Kaler, E. W.; Stradner, A.; Glatter, O. *J. Phys. Chem. B* **1998**, *102*, 3105–3113.

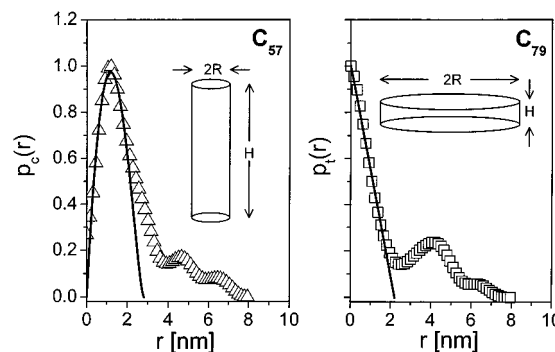


Figure 4. Cross-sectional pair distance distribution functions of complex C_{57} for cylindrical symmetry ($p_c(r)$, left-hand side) and of complex C_{79} for disklike symmetry ($p_d(r)$, right-hand side) according to eqs 3 and 4, respectively. The curves indicated by triangles and squares respectively, were calculated from the scattering data. The dashed lines represent the $p_c(r)$ of an idealized cylinder with a diameter of 3.0 nm (left-hand side) and the $p_d(r)$ of a disk with a height of 2.2 nm (right-hand side). The insets indicate idealized symmetries of the particles.

where $J_0(qr)$ is the Bessel function of zero order. Similarly, if we presume that the disk's diameter is much larger than its height, the cross-section distribution function of the disk^{20,21} $p_d(r)$ can be calculated by the inversion of

$$q^2 I(q) \propto \int_0^\infty p_d(r) \cos(qr) dr \quad (4)$$

The resulting $p_c(r)$ for complex C_{57} and the $p_d(r)$ of C_{79} are shown in Figure 4 (triangles and squares respectively). From these the diameter of the cylinders and the height of the disks can be determined with great accuracy. For idealized particle geometry the cross-section distribution functions can be calculated²¹ and compared with the experimental $p_c(r)$ and $p_d(r)$ as shown in Figure 4 (solid lines). The r value where $p_c(r) = 0$ indicates the largest distance inside the cross-section, i.e., the diameter of the cylinders.²¹ Similarly the zero in the $p_d(r)$ indicates the thickness of the disk or lamella. By fitting, we calculated the average cylinder radius to be 1.5 ± 0.1 nm and the average thickness of the disks to be 2.2 ± 0.2 nm. In can be seen that significant deviations from the idealized geometries are present in the cross section distribution functions at higher distances (two small maxima). The reason for this is not yet clear. Probably these deviations result from ionic surroundings of the particles that are formed by the carboxylic acid groups and the sodium counterions. The density of the particles is lower around the surfaces than it is at the core, which is assumed to be enriched in its fluorinated alkyl chains of the surfactant and therefore is of high density. However, it must be said that the reason for the minima can also be the presence of a certain amount of aggregates, which produce a side maximum at the core–core distance to the next neighbor. Furthermore, a multilayered structure of the cross section of the disk as an explanation for the minima is unlikely due to the small value of the cross-section (2.2 nm).

An idea of the internal particle structure gained from simple geometric considerations. The length of perfluorododecanoic acid with a fully extended chain is 1.7 nm as calculated in the same way as for perfluorinated acids.²² Such an all-trans conformation seems to be reasonable because of the stiffness of the fluorocarbon chain; this is in contrast to the flexibility of its hydrocarbon analogue. The lengths of the dodecanoic acid in its

(22) Burkitt, S. J.; Ottewill, R. H.; Hayter, J. B.; Ingram, B. T. *Colloid Polymer Sci.* **1987**, *265*, 619.

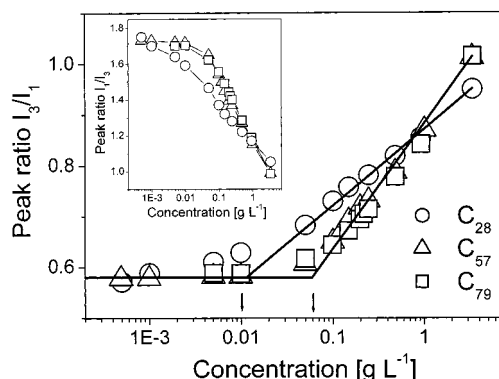


Figure 5. Plot of the peak ratio I_3/I_1 of the vibration fine structure for the emission of pyrene as a function of the logarithm of the concentration of the complexes C_{28} (circles), C_{57} (triangles), and C_{79} (squares). The straight lines are linear interpolations for the determination of the (cac)s that are indicated by arrows. For comparison, the inset shows a plot of the peak ratio I_1/I_3 as a function of the logarithm of the concentration of the complexes C_{28} (circles), C_{57} (triangles), and C_{79} (squares).

extended form (1.7 nm) is larger than the radius of the cylindrical particles (1.5 nm) and half of the height of the disklike particles (1.1 nm). Therefore, a partially interdigitated arrangement of the alkyl chains in the particles is probable.

The stability of the particles results from the interplay of ionic and hydrophobic interactions. Because they are chemically not cross-linked, it must be assumed that the particles dissolve at small concentrations. We used fluorescence spectroscopy as a sensitive method to determine their critical aggregation concentrations.

Pyrene Fluorescence. The fluorescence probe pyrene was added to the solutions of the nanoparticles and in order to obtain information on how the pyrene is located, steady-state fluorescence measurements were carried out. The $\pi \rightarrow \pi^*$ emission spectrum of the monomer pyrene exhibits five major vibration bands between 370 and 400 nm, labeled I–IV. The vibration bands I and III are located at wavelengths of 372.4 and 382.9 nm. It is known that peak 1 shows a significant decrease in its intensity compared with peak 3 when the polarity of the surroundings of the pyrene decrease. Thus, the ratio of the emission intensities of the vibration bands I and III (I_1/I_3) serve as a measure of the polarity of their surroundings. For example, the I_1/I_3 ratio is 0.58 in hexane and 1.87 in water.²³ Dipole-induced dipole interactions (Ham effect) between pyrene and its microenvironment are responsible for the changes in its intensity ratio I_1/I_3 .^{24,25} The I_1/I_{III} ratio of the nanoparticles as a function of the pH value is plotted in the inset of Figure 5.

The I_1/I_3 has its lowest values of about 1.0 at complex concentrations higher than 1 g L^{-1} where the nanoparticles are stable and the pyrene is located in the particles, which provide hydrophobic surroundings. We can estimate from this that the polarity of the pyrene surroundings in the particles is similar to *n*-pentanol in the pyrene scale.²³

The highest I_1/I_3 values of 1.75 are observed at concentrations smaller than 10^{-3} g L^{-1} , a value which is almost that of pyrene in water. There are obviously no hydrophobic surroundings available for the pyrene molecules at these small concentrations, and therefore the particles are obviously completely dissolved. It can be seen that the curve of C_{28} lies slightly below that of C_{57} and C_{79} , which are nearly identical. We interpret this minor difference as a result of the more hydrophobic character of the polymeric backbone of C_{28} . Similar curves for the complex particles have been reported recently by Lavasanifar et al.²⁶ for block copolymer micelles that form core-shell micelles with hydrophobic cores and hydrophilic shells. This is indicative for an analogy between the dissolution properties of our complex particles and micelles of special block copolymers that were designed for controlled release systems. Most likely, the complexes of polyampholytes have interesting properties for their development as drug carrier systems similar to the complexes of homopolymers.^{6,27} However, this will be investigated in a separated study.

The critical micell concentration (cac) is a characteristic value for polymer complexes similar to the critical micell concentration (cmc) of amphiphiles.²⁸ It is characteristic of cac, that the I_1/I_3 values start to decrease, or vice versa, the highest I_3/I_1 value starts to increase. It can be seen in Figure 5 that the I_3/I_1 increases discontinuously at 0.01 g L^{-1} for C_{28} and at 0.06 g L^{-1} for C_{57} and C_{79} . These values seem to be reasonable approximations of the cac of these complexes.

Conclusion

Discrete nanoparticles were prepared by using complexes of polyampholytes and perfluorododecanoic acid as a fluorinated lipid. The cationic groups of the polyampholytes were complexed by the fluorinated anionic amphiphiles to noncharged entities that aggregate and tend to show a phase separation. A macroscopic phase separation is prevented by the methacrylic acid and therefore stabilizes the particles ionically. The ζ potentials were found to be about -40 mV which gave a long-term stability to the particles of C_{57} and C_{79} . Small-angle X-ray scattering investigations reveal that the particles are anisotropic. They are disk-shaped when the cationic to anionic monomer ratio of the polyampholyte is high and cylindrically shaped when it is low. The possibility of producing different particle shape characteristics by simply changing the amount and ratio of cationic and anionic charges of the polyampholytes seems to be promising for nanoparticle design. For example, new drug carriers and target systems could be attractive applications.

However, intense investigations will be necessary to determine the quantitative relationship between the charge characteristics of the polyampholytes and the structure of nanoparticles formed of their complexes.

Acknowledgment. The financial support of the Deutsche Forschungsgemeinschaft (DFG-Schwerpunkt "Polyelektrolyte mit definierter Molekulararchitektur", Grants Lo418/7-1 and JA 555/6-1), the Max Planck Society, and the Fraunhofer Society is gratefully acknowledged.

LA020067V

(23) D. C. Dong, M. A. Winnik, The PY scale of solvent polarities—solvent effects on the vibronic fine-structure of pyrene. Fluorescence and empirical correlations with ET-value and Y-value. *Photochem. Photobiol.* **1982**, 35 (1), 17–21.

(24) R. C. Mast, L. V. Haynes, Use of fluorescent-probes perylene and magnesium 8-Anilinoanthracene-1-sulfonate to determine critical micelle concentration of surfactants in aqueous-solution. *J. Colloid Interface Sci.* **1975**, 53, 35–41.

(25) M. Hollas, M.-A. Chung, J. Adams, Complexation of pyrene by poly (allylamine) with pendant beta-cyclodextrin side groups. *J. Phys. Chem. B* **1998**, 102(16), 2947–2953.

(26) Lavasanifar, A.; Samuel, J.; Kwon, G. S. *Colloids Surf. B: Biointerfaces* **2001**, 22, 115–126.

(27) General, S.; Thünemann, A. F. *J. Pharm.* **2001**, 230, 11–24.

(28) Goddard E. D. *Colloids Surf.* **1986**, 19, 255.